

Understanding the Heat Transfer Characteristics and Axis Switching Phenomenon in High Aspect Ratio Elliptical Orifice Impinging Synthetic Jets



Pawan Sharma, Prakhar Bharadwaj, Kshitij Bhat, K. A. Vyvaswath, Bhavya Dalal, Pradeep K. Singh, Santosh K. Sahu, and Harekrishna Yadav

1 Introduction

Technological innovation in electronics is leading to smaller components with better performance and higher heat fluxes than ever before. As far as the reliability and optimum performance of these devices are concerned, the conventional cooling techniques are becoming inadequate for handling these intense heat fluxes. As a result, there is a need for compact and high-efficiency cooling devices. Impingement jets have attracted great interest recently for heat removal [1]. Impingement cooling at maximum flow speed is known to offer heat transfer coefficients up to three times that of conventional convective cooling [2]. Among impingement jet cooling methods, synthetic jet cooling has received significant attention because of the enhanced mixing due to its transient nature. SJs are found to be superior to continuous jets in terms of entrainment rate due to the rapid formation of periodic vertical structures in SJ [3]. Especially among SJs, the enhanced entrainment and mixing properties of Non-circular SJs are better than those of axisymmetric jets [4]. Synthetic Jet Actuators are novel active flow control zero-net-mass-flux (ZNMF) devices [1], i.e., the mass ejected by the actuator cavity during ejection is equal to the mass sucked during the suction stroke. SJs have significant momentum flux, i.e., there is a net-momentum addition due to the movement of the diaphragm. When an SJ is ejected through a non-axisymmetric orifice, the shape of the jet fluctuates as it flows downstream due to self-induced deformations of the vortex rings [5]. This phenomenon of the rotation of the jet shape in symmetric vortex rings is called axis

P. Sharma (✉) · P. Bharadwaj · K. Bhat · K. A. Vyvaswath · B. Dalal · P. K. Singh · S. K. Sahu · H. Yadav
Department of Mechanical Engineering, Indian Institute of Technology Indore, Indore 453552, India
e-mail: phd1901203008@iiti.ac.in

switching. This change in cross-section shape increases downstream, away from the jet origin. The shape change is such that the forms remain almost similar to the jet opening, with its major and minor axis rotated at angles concerning the jet origin. Axis switching is of great significance for heat transfer applications and has been observed in rectangular jets [6], elliptic jets [4, 7], and other more complicated non-circular jets [8, 9]. Depending on initial conditions at the jet inlet, the cross-section of non-circular jets can evolve in the expansion region of the jet between the orifice exit and the impingement plate [5, 6]. It takes place through shapes similar to that at the jet inlet, with its major and minor axis rotated at angles depending on the jet geometry.

2 Literature Review and Objective

Synthetic Jets (SJ) have a vast potential to meet the cooling demand for future electronic applications. The main advantages of SJ cooling are its simple structure, low weight, low power consumption, and its high reliability in operations without the need for a dedicated plumbing system, since SJs are generated directly from the ambient fluid [5]. Axis switching is a phenomenon that is extensively studied in the case of non-axisymmetric impingement jets. Reodikar et al. [10] considered compressible impingement jets from different orifice geometries to study the mechanism of axis switching and its influence on heat transfer characteristics. They found that the phenomenon of axis switching is prevalent in elliptic jets at low orifice-to-plate ratios ($z/D \approx 2$), and elliptic jets mostly undergo an axis switch of 90 degrees. At larger z/D values, they reported that the jet section becomes axisymmetric regardless of the initial shape or aspect ratio at the orifice exit. They attributed this phenomenon to differential velocity gradients and jet spreading. It is seen that most of the work on elliptic impingement jet cooling focuses on lower aspect ratios. Gutmark and Grinstein [10] reported that the evolution of the jets strongly depends on multiple initial conditions at the elliptic nozzle exit, such as thickness distribution at the nozzle lip, non-uniformity of shear-layer thickness, the eccentricity measured by the nozzle geometrical aspect ratio, and Reynolds and Mach numbers. Shi et al. [7] studied the influence of various initial conditions on the behavior of elliptic jets experimentally. With a laser-induced fluorescence and 2D stereoscopic particle image velocimetry, they concluded that the entrainment ability of the elliptical synthetic jet is greater than that of the circular synthetic jet and increases with the orifice aspect ratio ($AR \leq 4$) and Reynolds number. On the other hand, Reodikar et al. [9] reported that the heat transfer characteristics of circular and non-circular jets are comparable and observed a better performance for the case of circular jets in all conditions. In addition to this, Lee and Lee's [11] experimental study of local heat transfer distribution of elliptic impinging jet found that for higher orifice-to-plate distance ($z/D > 6$), the heat transfer rates of the elliptic impinging jet are lower than those for the circular jet in the stagnation region. They argued that the cause of this phenomenon is that, in the central area, most of the momentum of the elliptic jet is lost before arriving

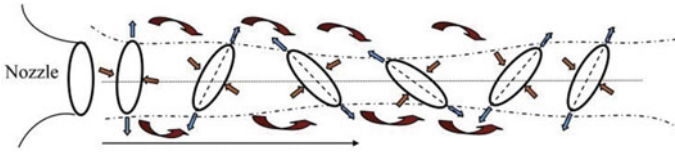


Fig. 1 Axis switching (Reodikar et al. [9])

at the impingement plate due to significant entrainment and substantial mixing with the ambient fluid. Additionally, they correlated the Nusselt number for the nozzle aspect ratio and the nozzle-to-plate spacing as $Nu \propto AR^{-0.082} z/D^{-0.077}$. Straccia and Farnsworth [6] studied the axis switching phenomenon for moderate orifice aspect ratios ($AR = 13, 19$) of a jet expelled from a synthetic jet actuator with a rectangular orifice. They used stereoscopic particle image velocimetry in addition to a Biot-Savart velocity induction solver to study the effect of orifice shape on vortex dynamics and axis switching. They reported that for $AR > 6$, the jet axis switched once and did not complete the axis switching cycle as opposed to jets with lower AR , which switched axis 2–3 times before the vortices lost coherence. They found a double peak in the mean jet centerline velocity profile, which became more prominent with increasing AR . A literature survey suggests a significant amount of studies on elliptic jet impingement. However, most studies consider only a lower aspect ratio ($AR < 4$) of an elliptic orifice. On the other hand, the effects of higher aspect ratios in rectangular orifices on impinging jets' dynamics and heat transfer characteristics have been studied in great detail. The objective of the present study is to investigate the influence of higher orifice aspect ratios ($AR = 10, 14$) on the axis switching behavior and the heat transfer characteristics of the elliptic jet. The present study experimentally analyzes the local and average Nu over the impingement plate and studies the temperature variation on the impingement plate (Fig. 1).

3 Materials and Methods

The experimental setup comprises a Synthetic Jet Actuator (SJA) assembly, hot-wire anemometry, an IR thermal imaging setup along with a heated foil, as shown in Fig. 2. The SJ actuator assembly uses a loudspeaker of 133 mm diaphragm size and a 15 mm diameter orifice plate ($t/d = 0.33$). A power oscillator (SI-28DR) supplies the input sinusoidal signal to the SJ actuator. The amplitude of the input signal is maintained constant ($= 4.5V_{rms}$). The frequency of SJ actuation is fixed as 40 Hz (i.e., its resonance frequency). A constant temperature hot-wire anemometer (Mini CTA 54 T42) with a single wire probe is employed to measure the flow velocity at the orifice exit. A 120×120 mm size matte finish test foil (SS material, AISI-304) is heated by a direct current power source for a constant heat flux of 2.5 kW/m^2 . The back side of the test surface is painted with flat black paint to achieve uniform emissivity ($\epsilon = 0.95$). The thermal imaging technique with an IR camera (FLIR:

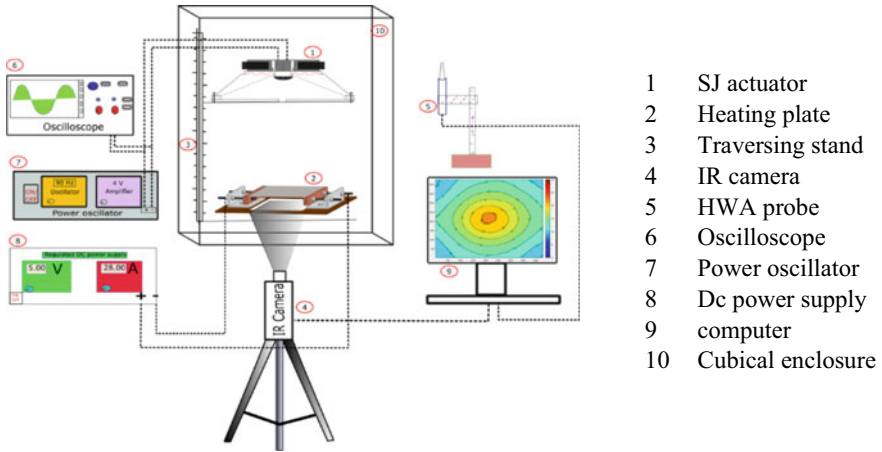


Fig. 2 Schematic of the experimental setup used in present investigation

A655sc) is used to study the heat transfer characteristics by gauging the temperature of the test surface. The IR camera measures temperatures from 0 to 2000 °C with an uncertainty of 1.5%. A calibration technique elaborated in [12] is employed to obtain the emissivity of 0.95 from the IR camera setup.

Apart from this, a stepper motor-controlled traversing stand is used to maintain the surface distance between the orifice plate and heated foil. All the experiments are conducted in an enclosed environment to abstain from surrounding effects. The ambient temperature (T_a) during the experimental investigation is measured with a pre-calibrated K-type thermocouple by placing it in the enclosed chamber of the experimental setup.

3.1 Data Reduction

The centerline mean velocity is measured by the instantaneous velocity during the ejection stroke (half cycle) calculated as follows

$$U_0 = \frac{1}{T} \int_0^{T/2} u(t) dt \quad (1)$$

The Reynolds number (Re) based on mean centerline velocity can be calculated as

$$Re = \frac{U_0 \times d}{\nu} \quad (2)$$

where d is the orifice diameter and ν is the kinematic viscosity of the fluid.

The Average Nusselt (Nu_{avg}) number is computed as follows:

$$Nu_{avg} = \frac{h_{avg} \times d}{k_f} \quad (3)$$

where, k_f is the thermal conductivity of fluid.

The average heat transfer coefficient (h_{avg}) can be calculated as

$$h_{avg} = \frac{q_{conv}}{(T_s - T_a)} \quad (4)$$

Here, T_s and T_a are the temperature of test foil and its ambience, respectively, while q_{conv} is the net heat supplied to the test specimen.

$$q_{conv} = q_j - q_{loss}; \quad q_j = \frac{V \times I}{A} \quad (5)$$

q_j , while q_{loss} denotes the total heat loss from the target surface. The net supplied heat flux (q_j) is calculated by the supplied voltage (V) and current (I) across the test foil.

The heat loss from the target surface is obtained by no-flow experiment [13] and the corresponding equation for heat loss w.r.t ($T_s - T_a$) is stated as below for $T_a = 32$ °C.

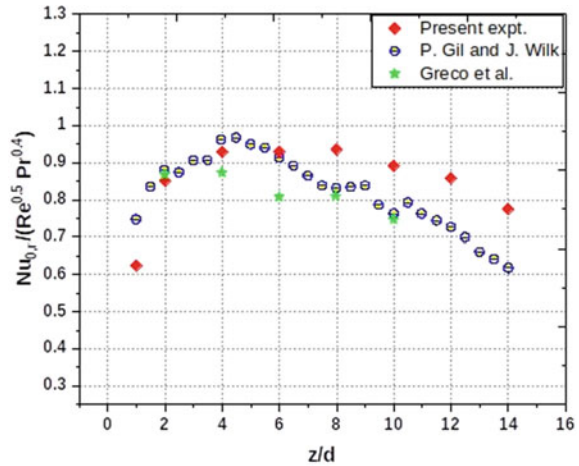
$$Q_{loss} = 0.23143 \times (T_s - T_a) - 0.31364 \quad (6)$$

A maximum of 21.1% heat loss is computed, which combines the heat loss due to natural convection and radiation from the foil surface (from both top and rear surface). The maximum uncertainty associated with q_{conv} and Nu_0 is found to be ± 3.95 and $\pm 4.53\%$, respectively as calculated based on Coleman and Steel [14].

4 Results and Discussion

In this section, heat transfer characteristics of the circular orifice ($AR = 1$) are compared to elliptical orifices ($AR = 10, 14$). All the orifices have the same effective orifice area among the studied orifices. The effective orifice diameter D is taken to be 15 mm based on our previous study [12], and the Reynolds number (Re) for the present investigation is calculated to be 8986.

Fig. 3 Results of reduced stagnation point Nusselt number as compared to the literature data



4.1 Validation Study

The results of heat transfer characteristics in the case of synthetic jet impingement cooling are compared to available literature data to evaluate the correctness of the experimental method. The reduced stagnation point Nusselt number ($Nu_{0,r}$) is considered for comparison to different experimental conditions. A 150 mm size diaphragm synthetic jet actuator with $V_{rms} = 1$ to 6 V, $Re = 3600$ to 22,950, and $L_0 = 0.84$ to 170.5 were used by Gil and Wilk [15]. In another study, Greco et al. [16] used an SJ actuator with a diaphragm size of 208 mm operating at $Re = 5250$ and $L_0/d = 5$ to 20. The current validation study employs a 133 mm diaphragm size actuator operating at $V_{rms} = 4$. The comparative heat transfer results are shown in Fig. 3 and the results closely match with the heat transfer results obtained by Gil and Wilk [15] and Greco et al. [16] (Fig. 4).

4.2 Effect of AR on Local and Average Nu

The distribution of local Nu on the heated surface is shown in Fig. 5a–d for different orifice-to-surface spacings ($z/d = 1, 3, 6, 10$). In Fig. 5a–d, local Nu is shown for orifices of different aspect Ratios (AR): $AR = 1$ (circular orifice) and $AR = 10, 14$ (elliptic orifice). The local Nu along the major and minor axis is plotted on the right and left side of the stagnation point, respectively, in each of the plots Fig. 5a–d. For all the orifices, the local Nu is observed to be largest at the stagnation point ($r/d = 0$), and then it decreases away from the stagnation point and reaches a local minimum at $r/d = 2.67$. For $z/D = 1$, a bell-shaped curve is observed for the case of $AR = 10$ on both the major and the minor axis. But such a shape of Nu is observed only on the major axis in the case of $AR = 14$. The Nu of $AR = 10$ and $AR = 14$ is higher than the

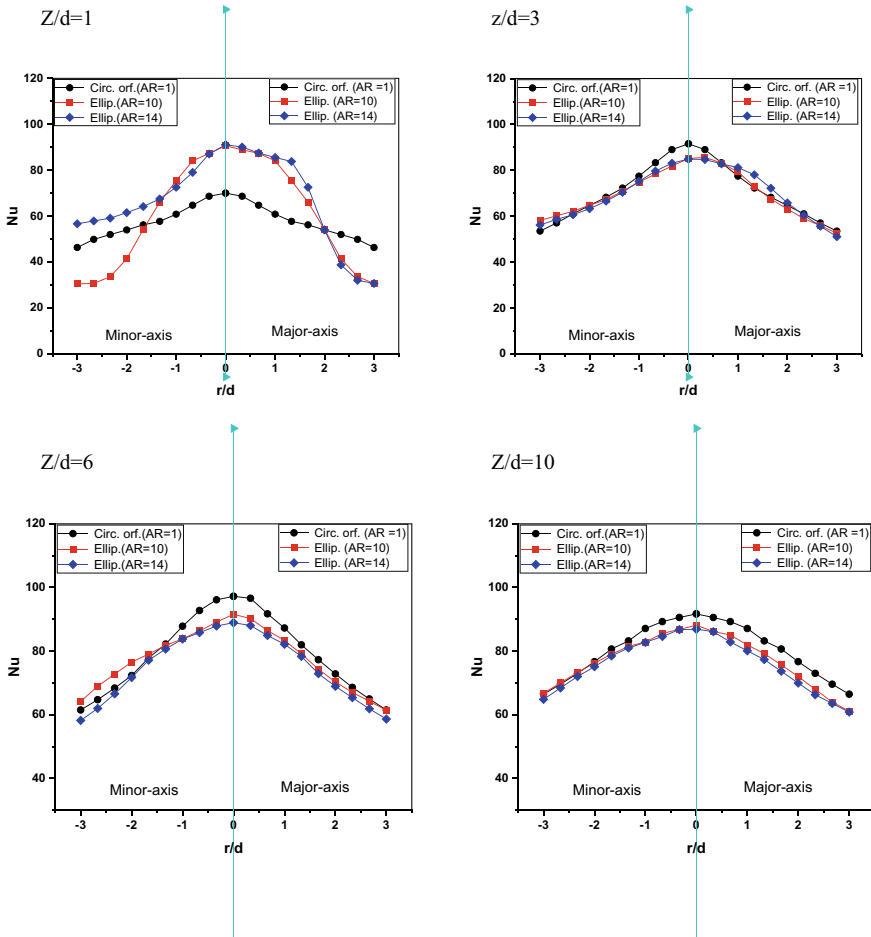


Fig. 4 Distribution of local Nusselt Number for various r/d and z/d values

Nu for circular orifice near the stagnation region, but the Nu for $AR = 10, 14$ is lower otherwise. High AR elliptic jets perform 28% better cooling in the near-field ($z/D = 1$). The Nu of $AR = 10$ and 14 has similar values closer to the stagnation region. For all the cases $z/D = 3, 6, 10$, the circular orifice performs better local cooling, as evident by a higher local Nu . In the case of far-field, The $AR = 10$ elliptic jet has higher Nu values than the jet with $AR = 14$ and thus, performs cooling better.

Figure 6 shows the line average Nusselt number (Nu_{l-avg}) variation on the Major (X) axis and Minor (Y) axis for the different aspect ratios ($AR = 1, 10, 14$) with the z/D values. The Nu_{l-avg} for the circular orifice ($AR = 1$) gradually increases and decreases after a certain point, whereas for elliptic orifices, a double peak is observed. Both plots show that, at low z/D values, Nu_{l-avg} is minimum. This is a consequence of low entrainment of surrounding air due to walling of the orifice and the heated surface.

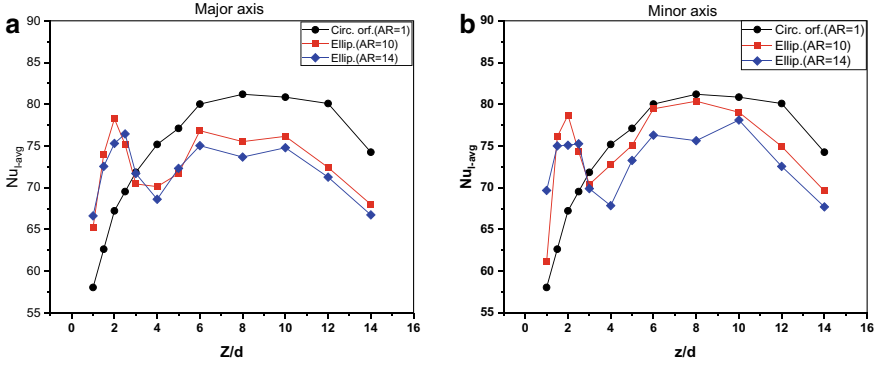


Fig. 5 Line average Nusselt number of studied orifices along **a** major axis, **b** minor axis

Additionally, at the near-field, the formed vortices fail to escape, and the recirculation decreases the heat transfer rate. However, for higher surface spacing ($z/D = 12$ to 14), Nu starts to decrease again due to a decrease in the kinetic energy and jet turbulence in the far-field region. So, the maximum heat transfer is obtained in the intermediate field ($z/d = 6$ to 10). The higher aspect ratio elliptic jets offer a higher Nu at lower z/D distances than circular orifices, similar to the findings of Bhapkar et al. [4]. This is due to the high spreading rate of elliptical orifices as compared to circular orifices. Among $AR = 10$ and 14 , the elliptic jet with $AR = 10$ performs better cooling than $AR = 14$, evident for the Nu_{l-avg} plots.

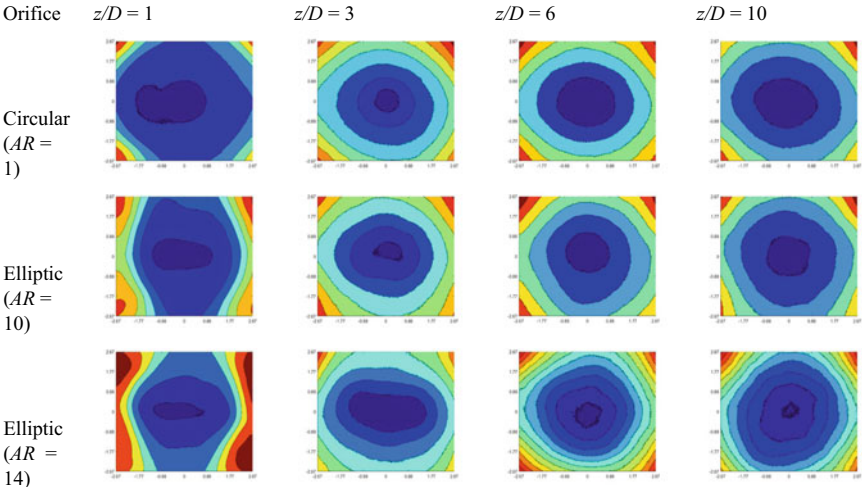


Fig. 6 Local temperature contour maps for different aspect ratios and orifice to surface distances

4.3 Axis Switching

In Fig. 5a,b, at the near-field ($z/D = 1,3$), the local Nu values for the major axis of the $AR = 14$ jet are higher than the minor axis Nu measurements. This suggests that the cooling is highly localized and similar to the shape of the orifice. This is also clearly apparent from the Fig. 6 showing IR thermography plots for $z/D = 1,3$ with $AR = 14$. As the jet progresses downstream, for values of $z/D = 6$ and 10 , the minor axis Nu values are slightly higher than the major axis plots. The IR thermography contour plots also depict a similar behavior. The heat transfer characteristics of the elliptic jets change with the axial distances. This suggests that axis switching is observed even in the case of higher AR elliptic jets.

5 Conclusion

This experimental study investigates the influence of the elliptic orifice aspect ratio on local heat transfer between a smooth flat plate and the impinging jet of air at different nozzle-to-plate distances. The following conclusions are drawn from this study:

1. Higher aspect ratio jets offer higher Nu values at low z/D values than axisymmetric orifices. For $z/D = 1$, elliptic jets offered 28% higher heat transfer rate in the stagnation region than the circular jet. Thus, high aspect ratio elliptic jets perform better cooling in the near-field region of the jet.
2. Circular jets produce a single peak in the Nu_{avg} vs. z/D plot, which lies in the mid-field region ($z/D = 6$ to 10). Contrary to this, elliptic jets ($AR = 10,14$) produce double peaks lying in near-field ($z/D = 1$ to 3) and mid-field regions ($z/D = 6$ to 10).
3. Axis switching is observed even for synthetic jets ejected from high aspect ratio ($AR = 10,14$) elliptic orifices.

Nomenclature

D	Orifice diameter[mm]
t	Orifice plate thickness[mm]
Nu	Nusselt Number
z/D	Dimensionless orifice to surface distance
r/D	Dimensionless radial distance
ε	Emissivity
Re	Reynolds number
V_{rms}	Root mean square amplitude [V]

T_s	Surface temperature of test foil [$^{\circ}\text{C}$]
T_a	Ambient temperature [$^{\circ}\text{C}$]
V	Voltage drop across foil [V]
I	Flowing current across foil [A]

References

1. Sharma P, Singh PK, Sahu SK, Yadav H (2021) A critical review on flow and heat transfer characteristics of synthetic jet. *Trans Indian Natl Acad Eng* [Internet]. Springer, pp 1–32. Retrieved from: <https://link.springer.com/article/https://doi.org/10.1007/s41403-021-00264-5>
2. Zuckerman N, Lior N (2006) Jet impingement heat transfer: physics, correlations, and numerical modeling. *Adv Heat Transf* 39
3. Smith BL, Glezer A (1998) The formation and evolution of synthetic jets. *Phys Fluids* 10:2281–2297
4. Bhapkar US, Srivastava A, Agrawal A (2014) Acoustic and heat transfer characteristics of an impinging elliptical synthetic jet generated by acoustic actuator. *Int J Heat Mass Transf Elsevier* 79:12–23
5. Gorman JM, Sparrow EM, Abraham JP (2014) Slot jet impingement heat transfer in the presence of jet-axis switching. *Int J Heat Mass Transf Pergamon* 78:50–57
6. Straccia JC, Farnsworth JAN (2021) Axis switching in low to moderate aspect ratio rectangular orifice synthetic jets. *Phys Rev Fluids Am Physic Soc* 6:1–26
7. Shi XD, Feng LH, Wang JJ (2019) Evolution of elliptic synthetic jets at low Reynolds number. *J Fluid Mech Cambridge Univ Press* 868:66–96
8. Zhong S, Garcillan L, Pokusevski Z, Wood NJ (2004) A PIV study of synthetic jets with different orifice shape and orientation. In: 2nd AIAA flow control conference, pp 1–13
9. Reodikar SA, Meena HC, Vinze R, Prabhu SV (2016) Influence of the orifice shape on the local heat transfer distribution and axis switching by compressible jets impinging on flat surface. *Int J Therm Sci Elsev Masson* 104:208–224
10. Gutmark EJ (1999) Flow control with noncircular jets. *Ann Rev Fluid Mech* [Internet]. 31:239–72. Retrieved from: <https://doi.org/10.1146/annurev.fluid.31.1.239>
11. Lee J, Lee SJ (2000) The effect of nozzle aspect ratio on stagnation region heat transfer characteristics of elliptic impinging jet. *Int J Heat Mass Transf* 43:555–575
12. Sharma P, Sahu SK, Yadav H (2022) Experimental investigation of flow and thermal characteristics of synthetic jet issuing from sharp- edged orifices. *Exp Heat Transf* [Internet]. Taylor & Francis, pp 1–25. Retrieved from: <https://doi.org/10.1080/08916152.2022.2105449>
13. Yogi K, Krishnan S, Prabhu SV (2021) Experimental investigation on the local heat transfer with an unconfined slot jet impinging on a metal foamed flat plate. *Int J Therm Sci* [Internet]. 169. Retrieved from: <https://www.sciencedirect.com/science/article/pii/S001793102033341X>
14. Coleman HW, Steele WG (2018) Experimentation, validation, and uncertainty analysis for engineers. John Wiley & Sons
15. Gil P Wilk J (2020) Heat transfer coefficients during the impingement cooling with the use of synthetic jet. *Int J Therm Sci Elsevier* 147:106132
16. Greco CS, Paolillo G, Ianiro A, Cardone G, de Luca L (2018) Effects of the stroke length and nozzle-to-plate distance on synthetic jet impingement heat transfer. *Int J Heat Mass Transf Elsevier* 117:1019–1031